



**HAL**  
open science

## Investigation on magnetic properties of mechanically alloyed $\tau$ -MnAlC with Fe addition

Van Tang Nguyen, Frédéric Mazaleyrat, Florent Calvayrac, Quang Minh Ngo, Nirina Randrianantoandro

► **To cite this version:**

Van Tang Nguyen, Frédéric Mazaleyrat, Florent Calvayrac, Quang Minh Ngo, Nirina Randrianantoandro. Investigation on magnetic properties of mechanically alloyed  $\tau$ -MnAlC with Fe addition. Journal of Magnetism and Magnetic Materials, 2021, pp.168892. 10.1016/j.jmmm.2021.168892 . hal-03454133

**HAL Id: hal-03454133**

**<https://univ-lemans.hal.science/hal-03454133>**

Submitted on 29 Nov 2021

**HAL** is a multi-disciplinary open access archive for the deposit and dissemination of scientific research documents, whether they are published or not. The documents may come from teaching and research institutions in France or abroad, or from public or private research centers.

L'archive ouverte pluridisciplinaire **HAL**, est destinée au dépôt et à la diffusion de documents scientifiques de niveau recherche, publiés ou non, émanant des établissements d'enseignement et de recherche français ou étrangers, des laboratoires publics ou privés.

# Investigation on magnetic properties of mechanically alloyed $\tau$ -MnAlC with Fe addition

Van Tang Nguyen<sup>a,b</sup>, Frédéric Mazaleyrat<sup>c</sup>, Florent Calvayrac<sup>d</sup>, Quang Minh Ngo<sup>a,b,e</sup>, Nirina Randrianantoandro<sup>d</sup>

<sup>a)</sup>University of Science and Technology of Hanoi, Vietnam Academy of Science and Technology, 18 Hoang Quoc Viet, Cau Giay, Hanoi, Vietnam

<sup>b)</sup>Graduate University of Science and Technology, Vietnam Academy of Science and Technology 18 Hoang Quoc Viet, Cau Giay, Hanoi, Vietnam

<sup>c)</sup>SATIE, CNRS, Université Paris-Saclay, ENS Paris-Saclay, 4 avenue des Sciences, 91190 Gif-sur-Yvette, France

<sup>d)</sup>Institut des Molécules et Matériaux du Mans – UMR CNRS n°6283, Le Mans Université, Avenue Olivier Messiaen, 72085 LE MANS Cedex 9

<sup>e)</sup>Institute of Materials Science, Vietnam Academy of Science and Technology, 18 Hoang Quoc Viet, Cau Giay, Hanoi, Vietnam

**Abstract.** *The influence of Fe addition on thermal stability, crystallography, and magnetic properties of  $\tau$ -Mn<sub>51</sub>Al<sub>47</sub>C<sub>2</sub> was investigated. Alloys with composition Mn<sub>51-x</sub>Fe<sub>x</sub>Al<sub>47</sub>C<sub>2</sub> (x= 0, 0.5, 1, 2, and 4) were synthesized by mechanical alloying method. High purity of  $\tau$ -Mn(Fe)AlC up to 98% could be obtained after 10h of milling, then annealed at 1050 °C for 1h, and followed by an aging process at appropriate temperatures from 515 to 540 °C for 50 minutes. It was found that the thermal stability of both  $\epsilon$  and  $\tau$  phases was enhanced by the addition of Fe up to 4 at.% into MnAlC alloy through a shifting of  $\epsilon$ -to- $\tau$  transformation temperature to high temperature region and a reduction in c/a ratio of Fe doped  $\tau$ -MnAlC compared to iron free  $\tau$ -MnAlC. While the magnetization and Curie temperature of Fe doped  $\tau$ -MnAlC showed a reduction compared to iron free  $\tau$ -Mn<sub>51</sub>Al<sub>47</sub>C<sub>2</sub>, coercivity seems not to be significantly affected. Ab initio calculation showed a lower magnetic moment of Fe ( $\mu_{\text{Fe}} = 1.77 \mu_{\text{B}}$ ) compared to Mn ( $\mu_{\text{Mn\_average}} = 2.36 \mu_{\text{B}}$ ) in  $\tau$ -Mn(Fe)AlC when Fe substituted Mn position at 1a site.*

Keywords: Mechanical alloying; Thermal Stability, Magnetic properties; MnFeAlC alloy

## I. Introduction

One of the current trends in permanent magnet is to find rare earth free magnets with properties between ferrite and rare earth magnets. Binary  $\tau$ -MnAl (crystal system: tetragonal, space group: P4/mmm) is known as a good candidate with a theoretical  $|BH|_{\max}$  of 112 kJ/m<sup>3</sup> [1]. Both Mn and Al are cheap and highly abundant on earth, which are needed in order to produce magnetic materials in a large scale and at a reasonable price. However,  $\tau$ -MnAl, which belongs to L1<sub>0</sub>-ordered magnets, is easily decomposed into non-magnetic phase at high temperature. In order to increase the stabilization of the  $\tau$ -MnAl phase, doping C is found to be effective [2, 3].

In ideal equiatomic  $\tau$ -Mn<sub>50</sub>Al<sub>50</sub>, Mn atoms occupy 1a site (0; 0; 0) while Al occupy 1d site (1/2; 1/2; 1/2) as shown in **Figure 1a**, in which Mn atoms at 1a sites have ferromagnetic coupling to each other. The Al planes are considered as a nonmagnetic layer as characteristics of L1<sub>0</sub>- ordered magnets. However, in reality, an excess of about 4 at.% Mn – which is necessary to form the  $\epsilon$ -MnAl precursor (crystal system: hexagonal, space group: P63/mmcE), in bulk material – enters the 1d sites, having antiferromagnetic coupling with neighboring Mn atoms at the 1a sites [4, 5] **Figure 1b**. As a consequence, it leads to a reduction of saturation magnetization ( $M_s$ ). Doping other elements that can replace the Mn or Al at 1d positions is therefore desirable in order to improve the magnetization, coercivity as well as other characteristics of the materials.

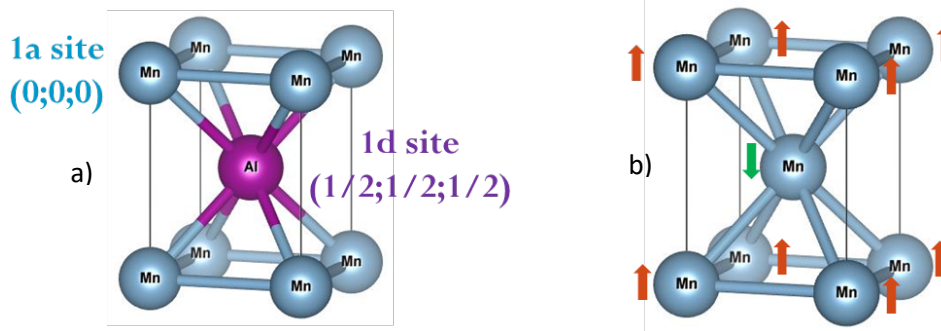


**Figure 1.** (a) Ideal equiatomic  $\tau$ -Mn<sub>50</sub>Al<sub>50</sub>, b)  $\tau$ -phase is obtained with an excess of Mn at 1d site (1/2;1/2;1/2) ( about 4 at.%) showing the antiferromagnetic coupling between Mn atoms at 1a and 1d sites.

Indeed, an enhancement in magnetization was reported by Matsumoto *et al.* and Sato *et al.* [6, 7] with low substitution of 3d transition metals (TMs) Fe, Co, Ni, or Cu on L1<sub>0</sub>-MnAl thin films. Among those, Fe was shown as a very promising candidate. In detail, Sato *et al.* reported that doping 2.5 at.% Fe enhanced nearly 12 % in  $M_s$  of  $\tau$ -MnAl [7]. while adding 5 at.% Fe improved approximately 1.7 times  $M_s$  [6]. The reason for the increase of magnetization in these thin films is attributed to the substitution of Mn atoms by other 3d TMs and consequently the expansion of lattice parameters of tetragonal structure of  $\tau$ -MnAl phase. However, the work carried out by [6, 7] was only on thin films, which is limited for permanent magnet applications.

Studies of doping 3d TMs, namely Cu, Ni, Co on bulk MnAl were also conducted, exposing many interesting results. Doping less than 2 at% Cu to bulk MnAl-C reported by J. Florian *et al.* showed an improvement in the extrinsic magnetic properties with die upsetting process [8]. However, doping more than 2 at% Cu led to a significant deterioration of the magnetic properties of  $\tau$ -MnAl as it decomposed into other non-magnetic phases [8]. Surprisingly, the addition of Cu did not affect the Curie temperature. More interestingly, although the addition of Ni or Co into  $\tau$ -MnAl did not improve the magnetic properties of  $\tau$ -MnAl phase, its thermal stability was enhanced, which is also an important factor for L1<sub>0</sub> ferromagnetic materials' application [9-11].

However, up to now, there is no experimental investigation on doping Fe to bulk MnAl(C) system. Theoretically, substitution of Mn by Fe up to 50 at.% on MnAl was studied extensively by first principle calculations, in which an opposite conclusion to the results achieved in thin films was given [12, 13]. It was shown that doping Fe deteriorates the magnetization of  $\tau$ -MnAl due to antiferro-magnetic intralayer exchange coupling created when Fe substitutes Mn or dilution effect that comes from the relatively smaller magnetic moment of Fe atom ( $1.9 \mu_B$ ) compared to Mn atom ( $2.45 \mu_B$ ) [12, 13]. Moreover, the effect of Fe addition on thermal stability of  $\epsilon$  or  $\tau$ -MnAlC was not researched in either thin films [6, 7] or bulk materials.

Therefore, in this paper we are going to present experimental results on the influence of Fe on thermal stability as well as the crystallography and magnetic properties of bulk  $\tau$ -MnAlC synthesized by mechanical alloying method, which was successfully used to achieve a very high purity of  $\tau$ -MnAlC in our previous work [14]. A theoretical calculation was also carried out in order to investigate the magnetic moments of different atoms in the material to support the experimental results.

## II. Materials and Methods

Manganese (99.95% in purity), iron (99.95 % in purity), aluminum (99.90 % in purity), and carbon (99.95% in purity) powders were weighted and mixed together. The nominal compositions  $Mn_{51-x}Fe_xAl_{47}C_2$  ( $x= 0, 0.5, 1, 2, 4,$ ) were studied. Balls to powder weight ratio was around 25:1. In this work we chose doping 2 at.% C in all samples as we found the best percentage to obtain high purity of  $\tau$ -MnAlC phase [14].

Planetary Micro Mill Pulverisette 7 premium line was deployed for milling process. The mixtures of powder were poured into the vials made of tungsten carbide and sealed within a glove-box filled with argon atmosphere in order to avoid oxidization. The obtained as-milled powder was recovered after 10h of milling at 400 rpm. The as-milled powder was then inserted into a quartz ampoule sealed under vacuum  $P = 10^{-4}$  Torr, and then put into a horizontal electric furnace (Elite) for annealing process at 1050 °C for 1h to obtain  $\epsilon$  phase and quenched in water. The annealed powder was aged at different temperatures to obtain  $\tau$  phase. Differential Scanning Spectrometer was used to determine the  $\epsilon$  to  $\tau$  transformation

temperatures. The X-ray diffraction measurements of Mn(Fe)AlC samples were conducted by PANalytical – X ray Diffractometer using  $\text{CuK}\alpha$  radiation. In order to clarify the effect of Fe on crystallography of MnAlC alloys, the phase identification and microstructure refinement were carried out by HighScore Plus and Maud software, respectively. Magnetic properties and Curie temperature ( $T_c$ ) of aged samples were measured by vibrating sample magnetometer (VSM) Lake Shore under maximum external magnetic field  $B = \mu_0 H = 2T$ . In addition, an ab initio calculation was carried out to calculate magnetic moments of Fe, Mn, and Al when Fe is substituted in 1a sites of  $\tau$ -MnAl by using WIEN2k. This software package is based on density functional theory (DFT), but uses the full-potential (linearized) augmented plane-wave ((L)APW) and local orbitals (lo) method [15, 16]. 1000 k-points, a muffin tin radius (RMT) of 2.5 a.u for Mn and 2.27 a.u for Fe and Al were utilized. The PBE density functional was used, a RMT\*KMAX (maximum plane waves) of 7 was chosen, and spin calculations as well as full spin orbit potentials were activated for all atoms.

### III. Results and discussion

#### 1. Crystallography and phase transformation

XRD diagrams of as milled, annealed Mn(Fe)AlC samples are depicted in Figure 2, and Figure 3, respectively. Figure 2 shows broadening peaks of  $\beta$  and high temperature  $\epsilon$  phase of all as milled samples, indicating the formation of very fine and short range ordered structure. None of Al or Fe peaks were detected. Notably, the high temperature  $\epsilon$  phase appeared as the result of solid reaction during the milling process.

Annealing at 1050 °C for 1h transformed the phases existing in the as milled samples to high temperature  $\epsilon$  phase Figure 3. However, the pure  $\epsilon$  phase could not be obtained in all samples. From 2 at.% Fe, the  $\gamma_2$  phase (crystal system: Rhombohedral, space group: R3m) appeared. It may indicate that the solubility of Fe in the  $\epsilon$  phase at the proposed composition is less than 2 at.%, which is comparable to the value obtained in case of Ni doping (1.5 - 2 at.% at 1100 °C) [9]. In addition to the  $\epsilon$  phase, detectable peaks of  $\text{Al}_2\text{O}_3$  were identified in all XRD patterns which come from oxidization of Al during milling or annealing processes.

In order to examine the effect of Fe doping on phase transformation and its stability, the DSC measurement of annealed Mn(Fe)AlC samples as well as the following aging process to obtain the  $\tau$  phase was conducted. Figure 4 depicts the obtained DSC curves, showing a single exothermic peak at each curve. The peaks correspond to the  $\epsilon$  to  $\tau$  phase transformation as being confirmed by the XRD diagrams of the samples after aging process at the peaks' temperature later on. It is noted that the annealed samples were aged at the temperature corresponding to the maximum of the exothermic peak (from 515 °C to 540 °C) in order to obtain the  $\tau$  phase. The XRD patterns of the aged samples are represented in Figure 5. Besides, in order to clarify the effect of Fe on crystallography of MnAlC alloys, phase identification and microstructure refinement were carried out by HighScore Plus [17] and Maud software [18], respectively. The results are summarized in Table 1. Note that the values Sig - Rwp show how good the refinement is. Good refinement is achieved when Sig < 2.0 and Rwp < 15. The evolution of lattice parameters a and c and c/a ratio of  $\tau$  phases are plotted in Figure 6.

From the DSC curves **Figure 4**, one can notice that there is a shift of the peaks to higher temperature region, which is demonstrated through the increment of  $T_{\text{peaks}}$ , showing an enhancement in thermal stability of the  $\epsilon$  phase, as also reported in case of doping Co and Ni [9, 10]. Furthermore, from the XRD diagram of aged samples, it is seen that the transformation from  $\epsilon$  phase to  $\tau$  phase was completed since the  $\epsilon$  phase no longer existed after the aging process. High purity of  $\tau$  phase up to 98% could be obtained in samples up to 2 at.% Fe (**Table 1**). Meanwhile, at 4 at.% Fe a lower 93% was achieved, in which a noticeable amount of  $\beta$  (crystal system: cubic, space group: P4132) and  $\gamma_2$  phase was observed. The reason for the appearance of  $\beta$  and  $\gamma_2$  phases at aged samples comes from the remaining  $\gamma_2$  phase that has already existed in the annealed samples and the fact that the  $\gamma_2$  phase is poor in Mn, therefore the remaining  $\epsilon$  phase of annealed samples becomes richer in Mn, consequently leading to the formation of  $\beta$  phase during the aging process. The improvement in thermal stability of  $\tau$ -MnAlC phase could be seen through the shrinkage of the unit cell volumes, more precisely the  $c/a$  ratio, displayed through its reduction tendency as more Fe was added (Figure 6). Indeed, among  $L1_0$  ferromagnetic materials, metastable  $\tau$ -MnAl has high  $c/a$  ratio ( $c/a \approx 1.3$ ) compared to other more stable ones, namely,  $L1_0$  – NiFe ( $c/a \approx 1$ ) [19],  $L1_0$  – CoPt ( $c/a \approx 0.97$ ) [20],  $L1_0$  – FePt ( $c/a \approx 0.96$ ) [21]. The reduction of  $c/a$  ratio that led to an improvement in thermal stability of  $\tau$ -MnAl is in agreement with the results and conclusion reported by [9, 10] when Ni and Co were added. In detail, in case of Ni doping, from up to nearly 2 at.% of Ni doping,  $c/a$  ratio decreased with an enhancement in thermal stability of  $\tau$ -MnAlNi alloy, whereas from 4 to 6 at.% of Ni doping, the thermal stability was reported to be decreased accompanied with an increase in  $c/a$  ratio [9]. In case of Co doping, the  $c/a$  ratio decreased monotonically from 1.285 of Co-free sample to 1.275 corresponding to 3 at.% of Co doping, being reported to strengthen the thermal stability of  $\tau$ -MnAlCo alloy [10].

Moreover, it can be deduced that the shrinkage of the lattice parameters means that Fe would rather substitute either Mn or Al atoms than stay at the interstitial sites within unit cell. Furthermore, since the empirical radius of Fe (126 pm) is smaller than that of Mn (127 pm) and Al (143 pm) [22], the reduction of lattice parameters are therefore understandable. In addition, if only the radius magnitudes of the atoms are concerned, one can see that the deviation in radii between Fe and Mn is clearly smaller than between Fe and Al; consequently, Fe should prefer to substitute the position of Mn than Al. In combination with the results of DSC, XRD and the calculated lattice parameters, one can emphasize that Fe was well dissolved into MnAlC crystal structure.

Doping Fe has a different effect on crystallite size of  $\epsilon$  and  $\tau$  phase (**Table 1**). While the crystallite size of  $\epsilon$  phase is relatively unchanged except for 4 at.% Fe; it decreases monotonically with  $\tau$  phase as Fe was added (**Table 1**). This behavior correlates to the presence of non-ferromagnetic phase in annealed sample, namely  $\gamma_2$  that account for approximately 5% in weight percentage of  $\text{Mn}_{47}\text{Fe}_4\text{Al}_{47}\text{C}_2$ ; and an increasing amount of both  $\gamma_2$  and  $\beta$  phases in aged samples. It is suggested that the presence of the mentioned non-ferromagnetic phases in annealed and aged samples may impede the extension of the crystallite growth of  $\epsilon$  and  $\tau$  phases.

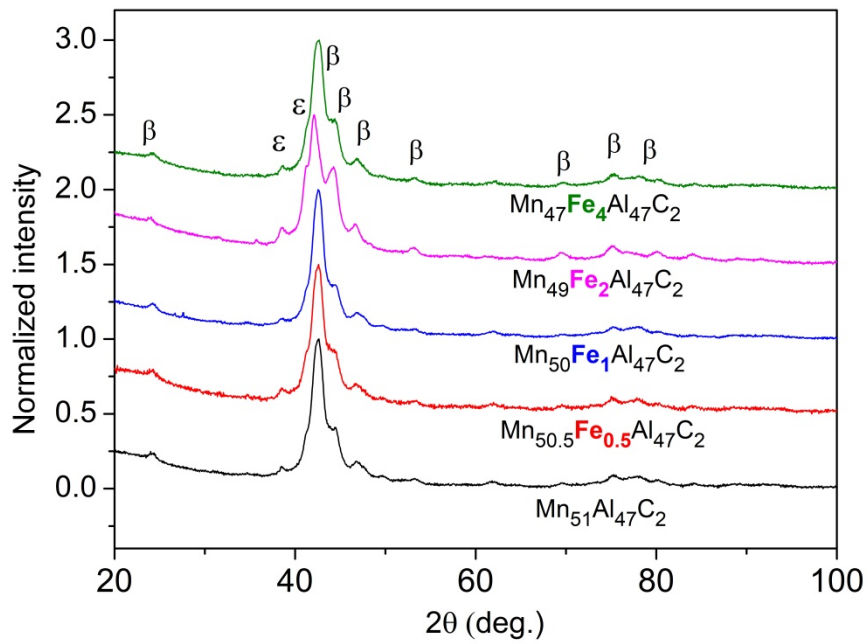


**Figure 2.** XRD diagram of as milled Mn(Fe)AlC.

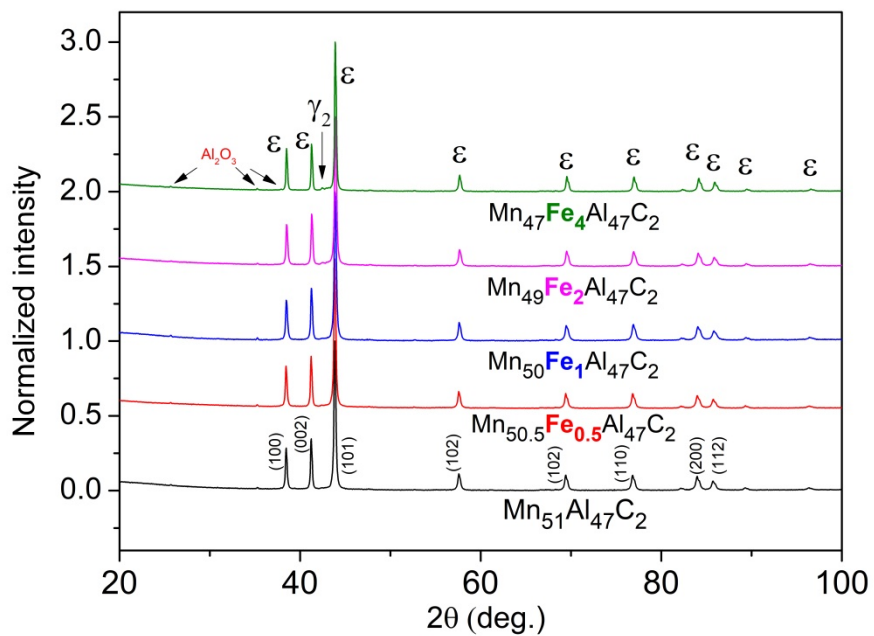


**Figure 3.** XRD diagrams of annealed Mn(Fe)AlC alloys.

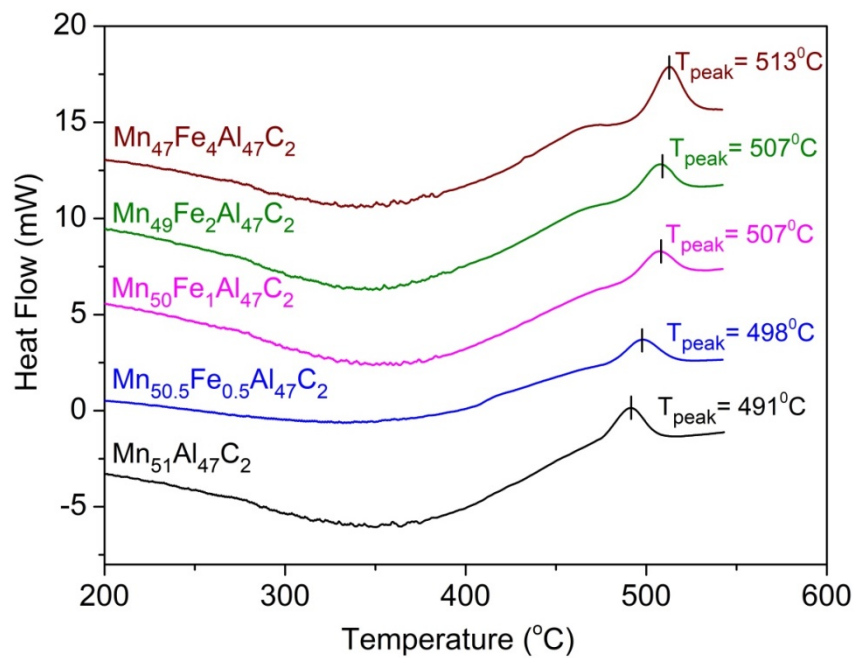


**Figure 4.** DSC curves of annealed Mn(Fe)AlC alloys

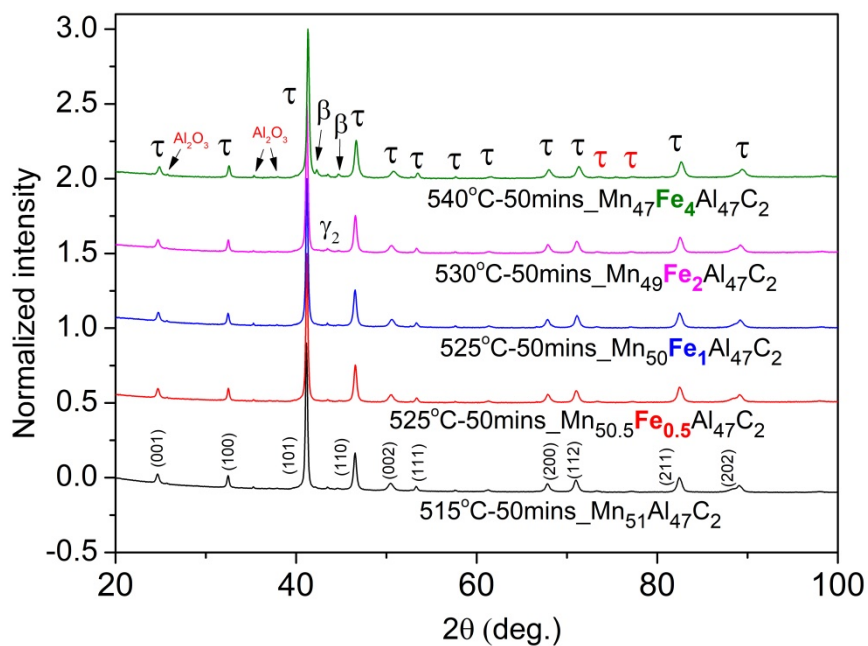


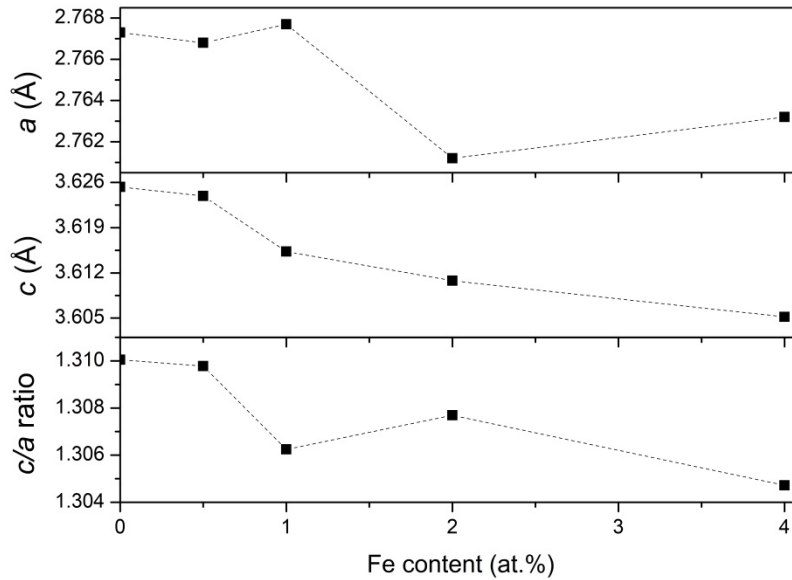
**Figure 5.** XRD diagrams of aged Mn(Fe)AlC alloys.

**Table 1.** Refined values of annealed and aged Mn(Fe)AlC alloys.

	$\epsilon$ -phase					$\tau$ -phase				
	CS (nm)	a (Å)	c (Å)	WP (%)	Sig-Rwp	CS (nm)	a (Å)	c (Å)	WP (%)	Sig-Rwp
Mn <sub>51</sub> Al <sub>47</sub> C <sub>2</sub>	106	<b>2.7107</b> ±0.0001	<b>4.3904</b> ±0.0002	98	1.63-1.45	81	<b>2.7673</b> ±0.0002	<b>3.6253</b> ±0.0002	98	1.87-1.66
Mn <sub>50.5</sub> Fe <sub>0.5</sub> Al <sub>47</sub> C <sub>2</sub>	104	<b>2.7096</b> ±0.0001	<b>4.3886</b> ±0.0002	98	1.67-1.34	81	<b>2.7668</b> ±0.0002	<b>3.6239</b> ±0.0004	98	1.92-1.61
Mn <sub>50</sub> Fe <sub>1</sub> Al <sub>47</sub> C <sub>2</sub>	112	<b>2.7081</b> ±0.0001	<b>4.3866</b> ±0.0003	98	1.85-1.45	79	<b>2.7677</b> ±0.0002	<b>3.6153</b> ±0.0003	98	1.81-1.41
Mn <sub>49</sub> Fe <sub>2</sub> Al <sub>47</sub> C <sub>2</sub>	103	2.7081 ±0.0002	<b>4.3866</b> ±0.0003	98	1.64-1.23	70	<b>2.7612</b> ±0.0002	<b>3.6108</b> ±0.0003	98	2.10-1.49
Mn <sub>47</sub> Fe <sub>4</sub> Al <sub>47</sub> C <sub>2</sub>	85	<b>2.7049</b> ±0.0001	<b>4.3819</b> ±0.0001	95	1.58-1.15	62	<b>2.7632</b> ±0.0002	<b>3.6052</b> ± 0.0004	93	1.74-1.32

CS: Crystallite size.

WP: Weight percentage.

**Figure 6.** Variation of a and c lattice parameters and c/a ratio of  $\tau$  phase on Fe content

## 2. Magnetic properties

### a. Hysteresis loops

Hysteresis loops obtained from VSM measurements of aged Mn(Fe)AlC alloys are depicted in **Figure 7**. The ferromagnetic characteristics are contributed from the  $\tau$  phase. One can see that the magnetization of all samples was not saturated under the applied magnetic field. Importation information including magnetization at 2T ( $M_{2T}$ ) and remanent magnetization ( $M_r$ ), coercivity ( $H_c$ ), which are extracted from the hysteresis, in relation with  $\tau$  phase content, and crystallite size are depicted in **Figure 8**, **Figure 9**, and **Figure 10**, respectively.

$M_{2T}$  and consequently  $M_r$  decreased as more Fe content was added, as shown in **Figure 8** and **Figure 9**, while the weight percentages of  $\tau$  phase up to 2 at. % Fe are relatively unchanged (**Table 1**). In

detail, a reduction of  $\approx 7.5\%$  in  $M_{2T}$  and  $\approx 6\%$  in  $M_T$  were observed at 2 at. % Fe compared with iron-free sample (Figure 8, Figure 9). According to the Bethe–Slater curve, interatomic distance between Mn atoms plays an important role in the exchange interaction, in which it can become ferromagnetic if the distance is expanded or antiferromagnetic if contracted [23]. Therefore, a reduction in lattice parameters (Table 1) when Fe was added into  $\tau$ -MnAlC alloys should be the reason for such decline in magnetization. Indeed, similar observation can be found when MnAl(C) was doped with different TM element such as Ni, Co, and Cu [8-10]. In addition, it is in accordance with the enhancement of  $M_s$  in case of Fe doped MnAl thin films when the lattice parameters increased to the optimal values [7]. The further expansion in the lattice parameters as reported by [7] led to the reduction of  $M_s$ , which is caused from a deterioration of the exchange interaction, which agrees with the Bethe – Slater curve [23].

Moreover, since Fe atom has its own magnetic moment, its orientation within the unit cell, its magnitude and how it interacts magnetically with Mn atoms could also contribute to the total magnetization. As mentioned before, the theoretical studies by [12, 13] indicated that dilution effect due to lower magnetic moment of Fe compared to Mn or antiferromagnetic exchange interaction between Fe and Mn atoms led to the deterioration of the magnetization. An experimental should be carried out in order to confirm this conclusion. For that, we have conducted Mossbauer spectrometric studies and the results will be published soon.

Above 2 at.% Fe, additional contribution of the lower content of  $\tau$  phase (Table 1) which was due to the appearance of  $\gamma_2$  and  $\beta$  phases (Figure 5), led to the apparent drop of  $M_{2T}$  and  $M_T$ .

The  $H_c$ , in contrast, did not show a monotonic increase or decrease. The deviation in  $H_c$  of Fe doped samples compared with iron-free sample is less than 3% (Figure 10). The relation of  $H_c$  to the crystallite size of  $\tau$  phase is also shown in Figure 10. It indicates that the reduction in the averaged crystallite size in the region from 81 nm to 62 nm seems not affect the behavior of  $H_c$  in such a manner that a decrease in crystallite size often lead to an increase in  $H_c$ . In fact, as was calculated in our previous publication [14], the maximum diameter of MnAl spherical particle that can be in the single domain region is 660 nm in diameter. Compared with the calculated average crystallite size of the  $\tau$  – Mn(Fe)AlC (Table 1), it suggests that the mode of magnetization reversal should be in the single domain region [24]. In addition, the maximum diameter of a spherical particle that can have coherent mode of spin reversal is:

$$d_{coh} = 2 \sqrt{\frac{24A}{\mu_0 M_s^2}} \quad (1)$$

where  $A$ ,  $\mu_0$ ,  $M_s$  are the exchange stiffness, the vacuum permeability, and the saturation magnetization, respectively [24]. If we take  $A \approx 10^{-11} \text{ Jm}^{-1}$  and  $M_s = 0.57 \text{ MA m}^{-1}$  [14], it yields  $d_{coh} \approx 48 \text{ nm}$ . This value is quite closed to our averaged crystallites size (Table 1), which means that the spin reversal is also near the coherent mode. In the report by [9], one can see that doing 0.6 at.% Ni into  $\tau$ -MnAlC alloys gave crystallite size of 108 nm lower than 138 nm of Ni free  $\tau$ -MnAlC; it did not result in an increase in  $H_c$ , but a decrease. For the thin films, the decay of  $H_c$  was observed in all elements doped to  $\tau$ -MnAl, which was explained by the degradation of the magnetocrytalline anisotropy originated from lattice changes or the presence of TM atoms themselves [7]. This explanation is in contrast with the results reported through first principle calculation by [12, 13], in which substituting up to 50 at.% Mn by Fe led to an increase of about 40% in anisotropy. It is noted that the calculation was assumed at 0 K and in our work the maximum doping percentage of Fe is less than 8%, so the effect as mentioned in the theoretical study if exists would not be significant.

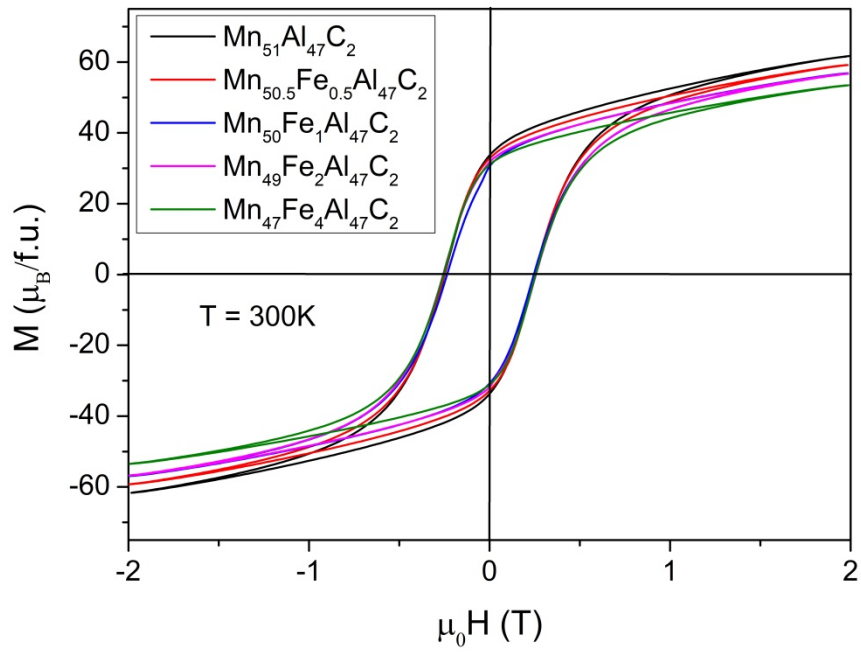


**Figure 7.** Hysteresis of aged Mn(Fe)AlC ferromagnetic alloys

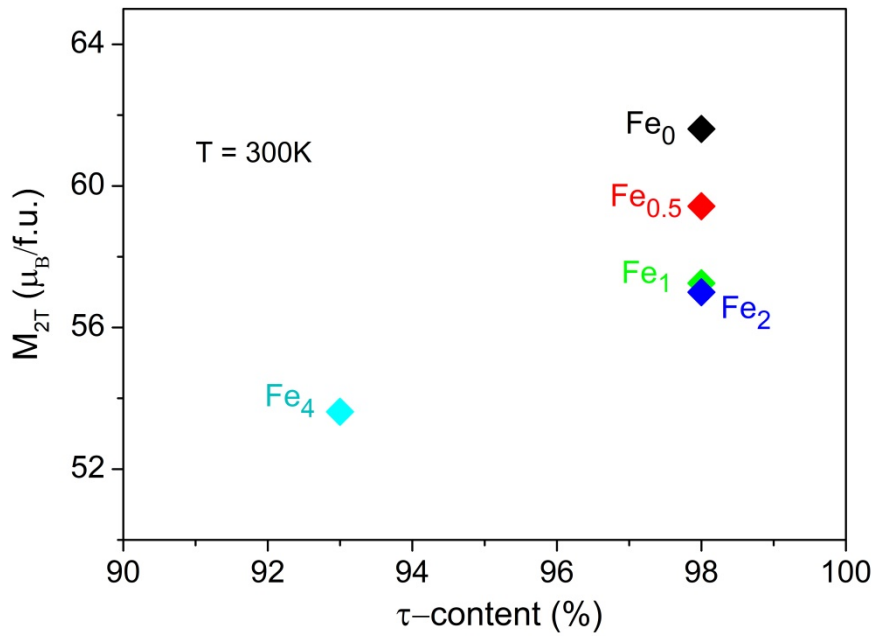


**Figure 8.** Magnetization at 2 T in relation with τ phase content of aged Mn(Fe)AlC.

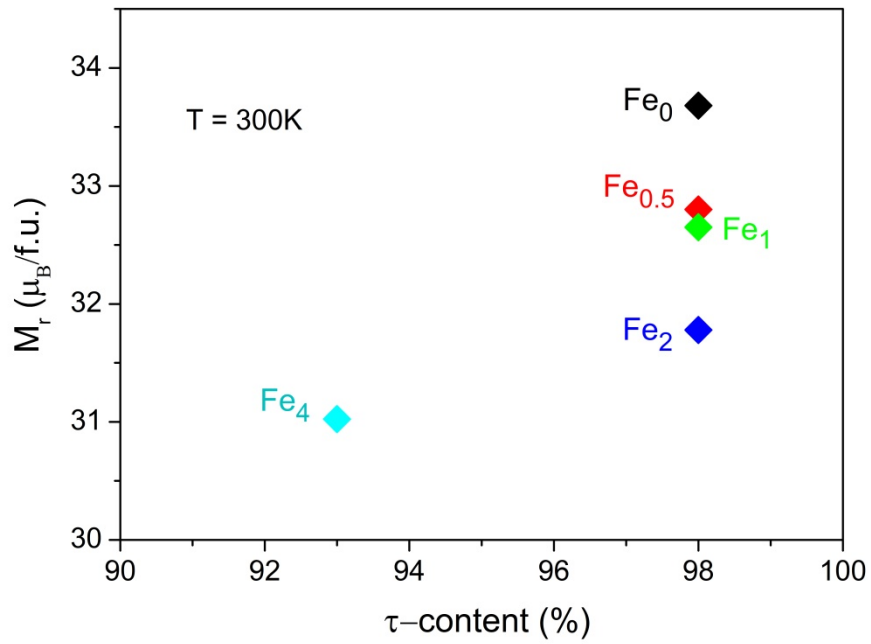


**Figure 9.** Remanent magnetization in relation with  $\tau$  phase content of aged Mn(Fe)AlC.

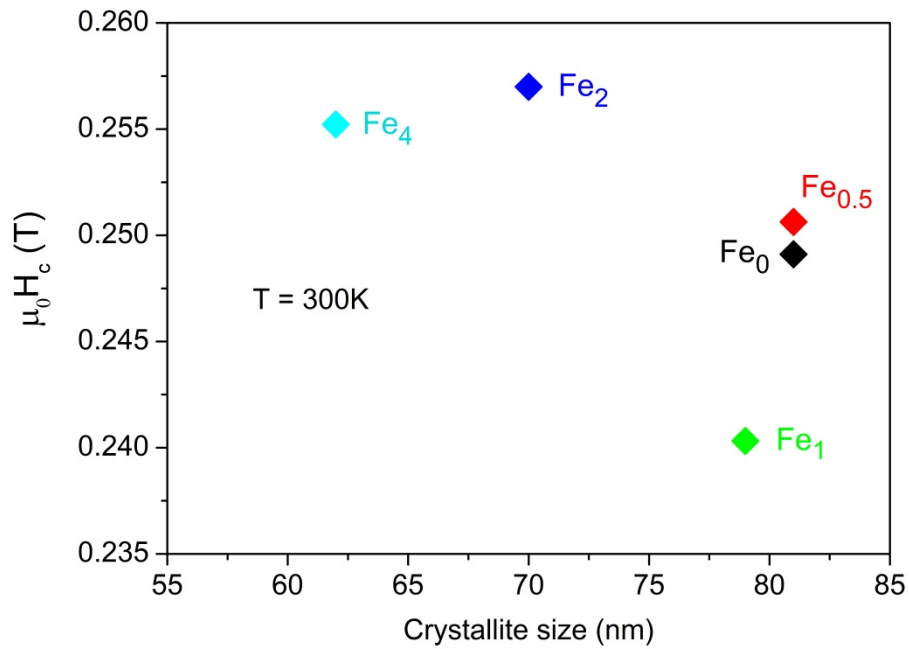


**Figure 10.** Coercivity of aged Mn(Fe)AlC alloys in relation with crystallite size.

### ***b. Thermomagnetic measurements***

The measured M-T curves of aged  $\text{Mn}_{51}\text{Al}_{47}\text{C}_2$ , aged  $\text{Mn}_{49}\text{Fe}_2\text{Al}_{47}\text{C}_2$ , and aged  $\text{Mn}_{47}\text{Fe}_4\text{Al}_{47}\text{C}_2$  are illustrated in **Figure 11**. The heating curves show Hopkinson peaks based on the Hopkinson effect when the sample are measured at low field (in this case 100 mT) [25]. By using the Hopkinson effect, it allows determining more precisely the value of  $T_c$ . In detail, the  $T_c$  was determined by drawing a tangent line at the slope where there is a sudden change in magnetization. The process is demonstrated in **Figure 11**,  $T_c$  is the intersection between the tangent line and the temperature axis. The  $T_c$  values of the aged samples are listed in **Table 2**. It is seen that the  $T_c$  is reduced from 568 K ( $\approx 295^\circ\text{C}$ ) to 551 K ( $\approx 278^\circ\text{C}$ ) when doping Fe up to 4 at.% into MnAlC alloy.

The decreasing of  $T_c$  may be explained through the relationship [23]:

$$T_c = \frac{2zS(S+1)J_{ex}}{3k_B} \quad (2)$$

where  $z$ ,  $J_{ex}$ ,  $S$ , and  $k_B$  are the coordination number, the exchange integral, the total spin, and the Boltzmann constant, respectively. According to this equation, the Curie temperature is proportional to the exchange integral and spin of Mn and Fe atoms. Therefore, the reduction in  $T_c$  is a good indication for the fact that adding Fe to Mn can deteriorate the exchange interaction and/or cause the dilution effect, which is resulted from Fe atoms having smaller magnetic moment compared to Mn atoms, as reported by the theoretical studies [12, 13]. For Ni doping [9], the  $T_c$  was found to be declined below 2 at.%. Above 4 at.% Ni, the  $T_c$  showed an augmentation, which is in coincidence with an appearance of  $\kappa$ -phase (crystal system: cubic, space group:  $Pm\bar{3}m$ ), another ferromagnetic phase of MnAl alloy [9].

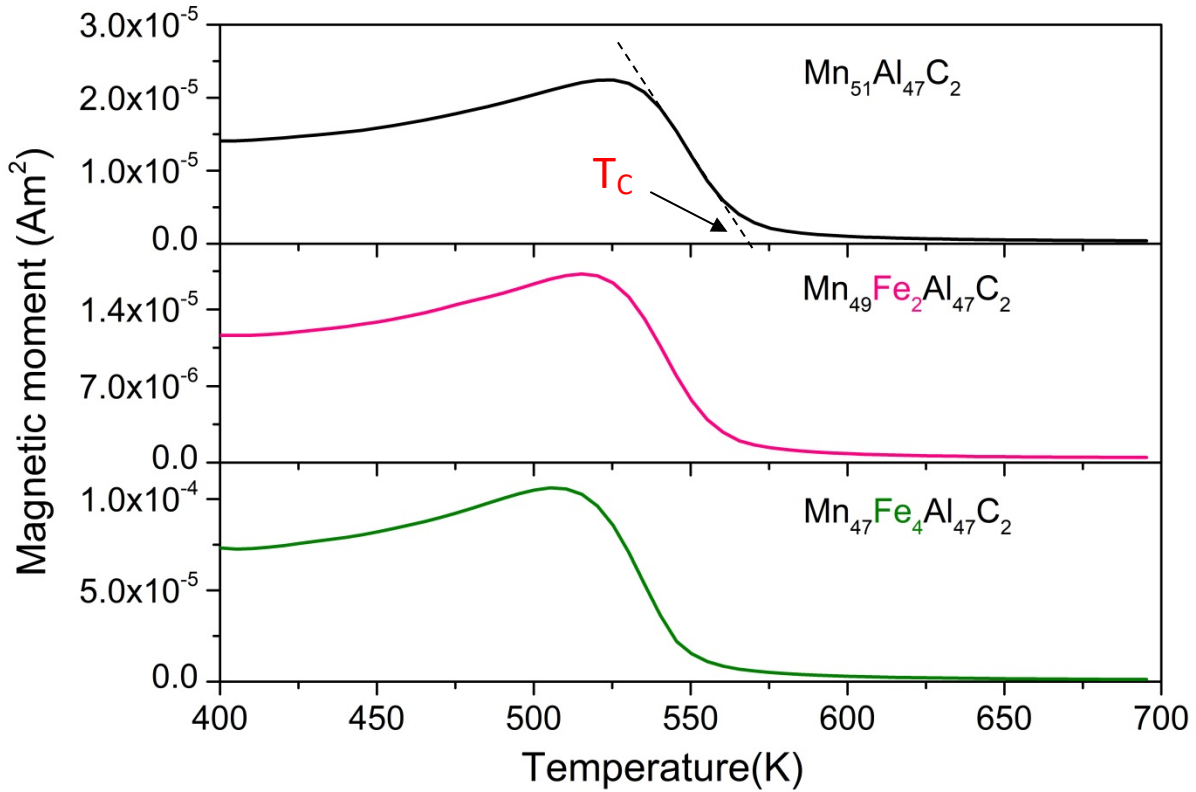


**Figure 11.** M-T curves on heating and cooling of aged  $\text{Mn}_{51}\text{Al}_{47}\text{C}_2$ , aged  $\text{Mn}_{49}\text{Fe}_2\text{Al}_{47}\text{C}_2$ , and aged  $\text{Mn}_{47}\text{Fe}_4\text{Al}_{47}\text{C}_2$ .

**Table 2.** Curie temperature of aged Mn(Fe)AlC samples.

Samples	$T_c$ (K)
Aged $\text{Mn}_{51}\text{Al}_{47}\text{C}_2$	$568 \pm 2$
Aged $\text{Mn}_{49}\text{Fe}_2\text{Al}_{47}\text{C}_2$	$561 \pm 2$
Aged $\text{Mn}_{47}\text{Fe}_4\text{Al}_{47}\text{C}_2$	$551 \pm 2$

### c. Ab initio calculation

The input configuration of MnFeAl supercell with 128 atoms, where one Fe atom substitutes one Mn atom at 1a site is demonstrated in [Figure 12](#). According to symmetry, the result gave 24 no-equivalent positions corresponding to 24 atoms ([Table 3](#)). As can be seen, the magnetic moment of Fe ( $\mu_{\text{Fe}} = 1.77 \mu_{\text{B}}$ ) is noticeably smaller than that of Mn ( $\mu_{\text{Mn\_average}} = 2.36 \mu_{\text{B}}$ ). The Al magnetic moments are small and contribute insignificantly to the total magnetization of the supercell. The magnetic moment of Mn in the calculation is in agreement with the empirical values ( $\mu_{\text{Mn}} \approx 2.4 \mu_{\text{B}}$  at 1a site) obtained by [26]. In addition, the magnetic moments obtained in our calculation are comparable with the values reported by [13], in which  $\mu_{\text{Fe}} = 1.9 \mu_{\text{B}}$ ,  $\mu_{\text{Mn}} = 2.45 \mu_{\text{B}}$  and  $\mu_{\text{Al}} \approx -0.06 \mu_{\text{B}}$ . It is noted that the calculation carried out by [13]

used the same assumption that Mn is substituted by Fe but using a different composition. If we only consider 100 atoms of  $\tau$  phase with 1 Fe atoms doped, which corresponds to 50 primitive cell of tau phase in the ab initio calculation, the total magnetization approximately equal to  $49 \times \mu_{\text{Mn\_average}} + \mu_{\text{Fe}} = 117.41 \mu_B$ . This value is much higher than the magnetization per formula unit of aged  $\text{Mn}_{50}\text{Fe}_1\text{Al}_{47}\text{C}_2$  ( $M_{2T} \approx 57.3 \mu_B/\text{f.u.}$ ). In fact this difference is understandable since the magnetization of aged  $\text{Mn}_{50}\text{Fe}_1\text{Al}_{47}\text{C}_2$  was not saturated under applied field 2T, there is a difference in lattice parameters between experimental  $\text{Mn}_{50}\text{Fe}_1\text{Al}_{47}\text{C}_2$  at 300K and at 0 K by ab initio calculation, and there is imperfection in real crystal structure like defects, grain boundaries and so on.

Moreover, noted that the proposal of dilution effect by [13] as mentioned above based on a statement of Curie temperature enhancement; therefore the idea of antiferromagnetic coupling between Mn and Fe was not supported by [13]. However, this is opposite to the results of  $T_c$  reduction measured in our work as described above. Therefore, the dilution effect that come from the lower magnetization of Fe compared to Mn should not be the only reason responsible for the reduction of magnetization in Fe doped  $\tau$ -MnAIC stated by [13], but also a possible deterioration of ferromagnetic exchange interaction within  $\tau$ -MnAIC alloys when Fe is added.

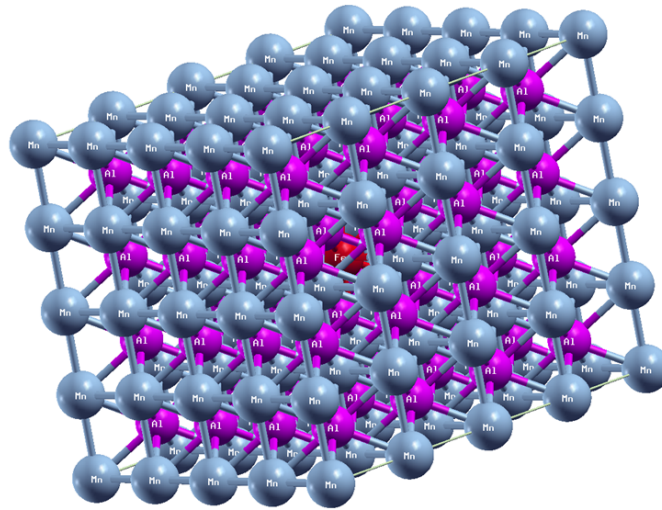


Figure 12. Input structure where Fe (red) substituted Mn atom.

Table 3. Values of magnetic moment calculated in MnAlFe by WIEN2K.

Atom type	Atom number	Magnetic moment ( $\mu_B$ )
Interstitial		0.07288
Mn	1	2.36073
Mn	2	2.36623
Mn	3	2.36536

Mn	4	2.36666
Mn	5	2.37533
Mn	6	2.34857
Mn	7	2.36146
Mn	8	2.36803
Mn	9	2.36828
Mn	10	2.37505
Mn	11	2.34849
Mn	12	2.39198
Mn	13	2.37244
Mn	14	2.36068
Mn	15	2.34449
Mn	16	2.36221
Mn	17	2.40622
Fe	18	1.77385
Al	19	-0.06610
Al	20	-0.06597
Al	21	-0.06622
Al	22	-0.06659
Al	23	-0.06668
Al	24	-0.06494
Total		146.77679

#### IV. CONCLUSIONS

$Mn_{51-x}Fe_xAl_{47}C_2$  ( $x= 0, 0.5, 1, 2,$  and  $4$ ) alloys were successfully synthesized by mechanical alloying method. High purity of  $\tau$ -Mn(Fe)AlC up to 98% was achieved. Fe atoms was found to be successfully dissolved into both  $\varepsilon$  and  $\tau$  -MnAlC crystal structure. The enhancement in thermal stability of both  $\varepsilon$  and  $\tau$  phases are displayed through the shifting of  $\varepsilon$ -to- $\tau$  transformation temperature to higher temperature region and the shrinkage tendency of the c/a ratio of  $\tau$ -Mn(Fe)AlC.

Adding Fe has an evident effect on the magnetization of  $\tau$ -MnAlC alloy. In detail, a reduction of  $\sim 7.5$  % in  $M_{2T}$  and  $\sim 6$  % in  $M_r$  observed at 2 at. % Fe compared to that of iron free sample even when the  $\tau$  phase content was approximately unchanged ( $\sim 98$  %). In contrast,  $H_c$  did not demonstrate a significant influence from Fe addition, showing variation of less than 3% of its magnitude. The  $T_C$  of Fe doped  $\tau$ -MnAlC was reduced compared to iron free  $\tau$ -Mn<sub>51</sub>Al<sub>47</sub>C<sub>2</sub>. The ab initio calculation showed that Fe possesses a smaller magnetic moment ( $\mu_{Fe} = 1.77 \mu_B$ ) compared to Mn ( $\mu_{Mn\_average} = 2.36 \mu_B$ ), which in combination with the reduction of  $T_c$  indicate that the decline of magnetization values may come from

both degradation of ferromagnetic exchange interaction, and the dilution effect originated from the lower magnetic moment of Fe compared to Mn.

## ACKNOWLEDGEMENTS

This work was supported by University of Science and Technology of Hanoi through research grant Ref. USTH.AE.02/20-21 and Graduate University of Science and Technology under grant number GUST.STS.ĐT2020-KHVL05.

## REFERENCES

- [1] J.M.D. Coey, Permanent magnets: Plugging the gap, *Scripta Materialia*, 67 (2012) 524-529.
- [2] Q. Zeng, I. Baker, J. Cui, Z. Yan, Structural and magnetic properties of nanostructured Mn–Al–C magnetic materials, *Journal of Magnetism and Magnetic Materials*, 308 (2007) 214-226.
- [3] Z. Liu, C. Chen, Z. Zheng, B. Tan, R.V. Ramanujan, Phase transitions and hard magnetic properties for rapidly solidified MnAl alloys doped with C, B, and rare earth elements, *Journal of Materials Science*, 47 (2012) 2333-2338.
- [4] H. Kōno, On the ferromagnetic phase in manganese-aluminum system, *Journal of the Physical Society of Japan*, 13 (1958) 1444-1451.
- [5] A. Koch, P. Hokkeling, M. vd Steeg, K. De Vos, New material for permanent magnets on a base of Mn and Al, *Journal of Applied Physics*, 31 (1960) S75-S77.
- [6] M. Matsumoto, A. Morisako, J. Ohshima, Properties of ferromagnetic MnAl thin films with additives, *Journal of Applied Physics*, 69 (1991) 5172-5174.
- [7] T. Sato, T. Ohsuna, Y. Kaneko, Enhanced saturation magnetization in perpendicular L10–MnAl films upon low substitution of Mn by 3 d transition metals, *Journal of Applied Physics*, 120 (2016) 243903.
- [8] J. Florian, F. Jens, N. Kornelius, T.G. Woodcock, The Influence of Cu-Additions on the Microstructure, Mechanical and Magnetic Properties of MnAl-C Alloys, *Scientific Reports (Nature Publisher Group)*, 10 (2020).
- [9] L. Feng, K. Nielsch, T.G. Woodcock, Enhanced Thermal Stability of the  $\tau$ -Phase in MnAl-C Alloys with Ni Additions, *Journal of Alloys and Compounds*, (2021) 159554.
- [10] Z. Xiang, Y. Song, B. Deng, E. Cui, L. Yu, W. Lu, Enhanced formation and improved thermal stability of ferromagnetic  $\tau$  phase in nanocrystalline Mn<sub>55</sub>Al<sub>45</sub> alloys by Co addition, *Journal of Alloys and Compounds*, 783 (2019) 416-422.
- [11] S. Mican, D. Benea, R. Hirian, R. Gavrea, O. Isnard, V. Pop, M. Coldea, Structural, electronic and magnetic properties of the Mn<sub>50</sub>Al<sub>46</sub>Ni<sub>4</sub> alloy, *Journal of Magnetism and Magnetic Materials*, 401 (2016) 841-847.
- [12] P. Manchanda, P. Kumar, A. Kashyap, M. Lucis, J.E. Shield, A. Mubarak, J. Goldstein, S. Constantinides, K. Barmak, L. Lewis, Intrinsic Properties of Fe-Substituted L10 Magnets, *IEEE Transactions on Magnetics*, 49 (2013) 5194-5198.
- [13] P. Manchanda, A. Kashyap, J.E. Shield, L. Lewis, R. Skomski, Magnetic properties of Fe-doped MnAl, *Journal of Magnetism and Magnetic Materials*, 365 (2014) 88-92.
- [14] N. Van Tang, F. Calvayrac, A. Bajorek, N. Randrianantoandro, Mechanical alloying and theoretical studies of MnAl (C) magnets, *Journal of Magnetism and Magnetic Materials*, 462 (2018) 96-104.
- [15] D. Singh, Plane waves, pseudopotential and the LAPW method. Boston, Dordrecht, in, London: Kluwer Academic Publishers, 1994.
- [16] E. Sjöstedt, L. Nordström, D. Singh, An alternative way of linearizing the augmented plane-wave method, *Solid state communications*, 114 (2000) 15-20.
- [17] M.S. T. Degen, E. Bron, U. König, G. Nénert, The HighScore suite, in: *Powder Diffraction December 2014*, pp. S13-S18.

- [18] L. Lutterotti, R. Camprostrini, S. Gialanella, R. Di Maggio, Microstructural characterisation of amorphous and nanocrystalline structures through diffraction methods, in: *Materials Science Forum*, Trans Tech Publ, 2000, pp. 657-664.
- [19] Y. Geng, *Microstructure and Magnetic Behavior Studies of Processing-controlled and Composition-modified Fe-Ni and Mn-Al Alloys*, in, University of Nebraska-Lincoln, 2014.
- [20] W.B. Pearson, *A handbook of lattice spacings and structures of metals and alloys: International series of monographs on metal physics and physical metallurgy*, Vol. 4, Elsevier, 2013.
- [21] M. Futamoto, M. Nakamura, M. Ohtake, N. Inaba, T. Shimotsu, Growth of L10-ordered crystal in FePt and FePd thin films on MgO(001) substrate, 6 (2016) 085302.
- [22] A.F. Wells, *Structural inorganic chemistry*, Oxford university press, 2012.
- [23] B. D. Cullity, C.D. Graham, *Introduction to Magnetic Materials*, Wiley-IEEE Press, 2008.
- [24] J.M.D. Coey, *Magnetism and magnetic materials*, Cambridge University Press, 2010.
- [25] J. Hopkinson, XIV. Magnetic and other Physical Properties of Iron at a High Temperature, *Phil. Mag.*, (1874).
- [26] M. Tyrman, A. Pasko, L. Perrière, V. Etgens, O. Isnard, F. Mazaleyrat, Effect of Carbon Addition on Magnetic Order in Mn-Al-C Alloys, *IEEE Transactions on Magnetics*, 53 (2017) 1-6.